Vertically Integrated Amorphous Silicon Color Sensor Arrays

Dietmar Knipp, *Member, IEEE*, Robert A. Street, Helmut Stiebig, Mathias Krause, Jeng-Ping Lu, Steve Ready, and Jackson Ho

***Abstract*—Large-area color sensor arrays based on vertically integrated thin-film sensors were realized. The complete color information of each color pixel is detected at the same position of the sensor array without using optical filters. Sensor arrays consist of amorphous silicon thin-film color sensors integrated on top of amorphous silicon readout transistors. The spectral sensitivity of the sensors is controlled by the applied bias voltage. The operating principle of the color sensor arrays and the influence of device design on spectral sensitivity are described. Furthermore, the image quality of the sensor arrays is analyzed by measurements of the line spread function and the modulation transfer function.**

***Index Terms*—Amorphous silicon, color sensor, optical sensor, thin film electronics.**

I. Introduction

IMAGING is usually performed by an array of sensor elements in combination with a color filter array (CFA). The CFA consists of a spatial arrangement of optical filters integrated on top of sensor elements. The most popular filter configuration is the Bayer filter configuration, which consists of $1\times$ filter for red, $2\times$ filters for green, and $1\times$ filter for blue [1], [2]. Therefore, four chromatic color pixels are required to form a color pixel. Furthermore, color detection using CFAs leads to color Moiré or color aliasing effects, which are observed when structures with high spatial frequencies are captured.

To avoid color aliasing effects and to increase the resolution of existing color sensor arrays, vertically integrated sensors have been proposed and realized. Here, color information is detected in the depth of the sensor. To illustrate the operating principle of the vertically integrated sensor, an image detection sequence is shown in Fig. 1. The vertically integrated sensor is compared with sensor arrays using a Bayer CFA. To illustrate the operating principle, an edge was projected on both sensor structures. Due to the finite size of the sensor pixels, aliasing effects are observed for both structures. However, for the vertically integrated sensor, only black and white aliasing is observed, whereas black and white aliasing plus color aliasing is observed for the sensor using a CFA. The reconstructed image for the two different sensor technologies is shown in Fig. 1(c). The colors detected at the edges of the projected image are distorted. In the case of a black and white edge projected on the Bayer-filter-based sensor array, colors are detected although the projected image is colorless.

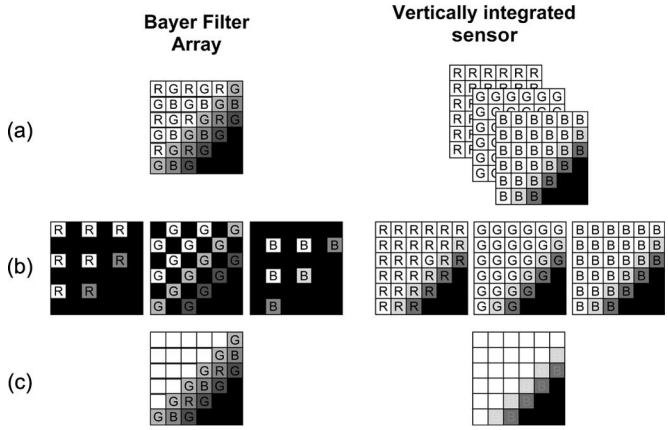

Fig. 1. Schematically illustrated edge detection of a sensor using a CFA and a vertically integrated sensor. (a) Black and white image of an edge projected on the CFA and the vertically integrated sensor. (b) RGB images of the projected image. (c) Resulting image of the projected edge.

Various vertically integrated sensor structures were realized by using different materials, design concepts, and contact configurations [3]–[11]. The wavelength-dependent absorption of the applied semiconductor material leads to the absorption of photons at various depths, so color information can be detected in the depth of the device. The suggested sensors range from two-terminal devices, which change their spectral sensitivity by varying the applied bias voltage [6]–[11], to vertically stacked diodes [3]–[5].

In terms of materials, most of the devices were realized by using crystalline or amorphous silicon and related alloys. These semiconductors are perfectly suitable for color sensor applications as these materials exhibit a strong wavelength-dependent absorption. In the case of crystalline silicon, sensors based on three vertically integrated p-n junctions were developed. Sensor arrays with a resolution of 10.6 megapixels were realized [3]. Due to the relatively small optical bandgap of crystalline silicon (1.14 eV), an elaborate optical design of stacked diodes is needed to match the spectral sensitivity of the sensor with the sensitivity of the human eye [2]. Nevertheless,

Manuscript received March 22, 2006. The review of this paper was arranged by Editor J. Hynecek.

D. Knipp is with the Electronic Materials and Devices Laboratory, Palo Alto Research Center, Palo Alto, CA 94304 USA, and also with the Department of Science and Engineering, International University Bremen, Bremen 28759, Germany.

R. A. Street, J.-P. Lu, S. Ready, and J. Ho are with the Electronic Materials and Devices Laboratory, Palo Alto Research Center, Palo Alto, CA 94304 USA.

H. Stiebig is with the Institute of Photovoltaics, Research Center Jülich, Jülich 52425, Germany.

M. Krause was with the Institute of Photovoltaics, Research Center Jülich, Jülich 52425, Germany. He is now with Infineon Technologies AG Dresden, Memory Products/Technology Center, Dresden 01099, Germany.

Digital Object Identifier 10.1109/TED.2006.875822

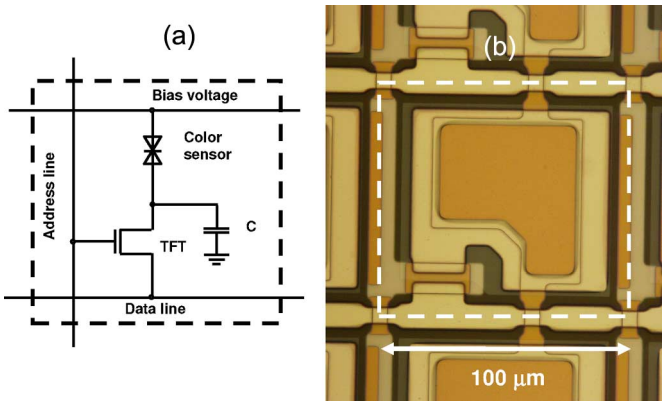

Fig. 2. (a) Pixel circuit and (b) photograph of a sensor pixel of a large-area color sensor array. (Color version available online at http://ieeexplore.ieee.org.)

stacked color sensors with color errors comparable to CFA-based sensor arrays were realized [12].

The optical bandgap of amorphous silicon is larger than the bandgap of crystalline silicon. The bandgap of an amorphous material is closer to the optical spectrum of the visible light, which recommends the material for optical sensor applications in the visible spectrum. Furthermore, amorphous silicon can be prepared at low deposition temperatures, which facilitates the realization of color sensors on top of an amorphous or crystalline readout electronics. The concept of vertically integrated sensors on a crystalline silicon readout electronic is known as thin film on application-specified integrated circuit (ASIC) (TFA) technology [13]. Sensor arrays with a resolution of 100 000 pixels were developed [14], [15]. Furthermore, amorphous silicon can be prepared on large areas, which facilitates the realization of large-area color sensor arrays. Although the color Moiré effect is getting more pronounced for larger pixels, the realization of large-area sensor arrays using vertically integrated three-color sensors has not been demonstrated.

In this paper, we present thin-film sensor arrays consisting of vertically integrated amorphous three-color sensors in combination with amorphous silicon thin-film readout electronics. To our knowledge, this is the first time that such a color Moiré-free large-area sensor array was realized. The entire sensor array is realized on a glass substrate at low temperatures using a plasma-enhanced chemical vapor deposition (PECVD) process. After a brief description of the sensor concept and the fabrication of the sensor array, the experimental results of the sensor arrays will be presented. In particular, the influence of the device design of the color sensor on the overall performance of the sensor array will be discussed.

II. Experiment

The sensor arrays were fabricated by PECVD at temperatures below 300 °C on 4-in glass wafers. The sensor arrays have a resolution of 512 × 512 pixels. Pixel addressing is realized by amorphous silicon thin-film transistors (TFTs). Each pixel contains a TFT, a storage capacitor, a color sensor, an address line, and a data line connecting the pixel with the external electronics. A pixel circuit of the sensor array is shown in Fig. 2(a). During operation, the address line is enabled so that

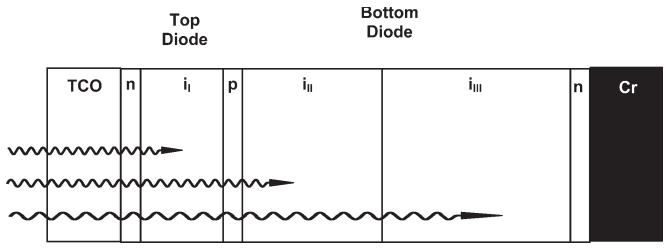

Fig. 3. Schematic band structure of the nipin sensor.

the photo-generated charge created in the sensor and stored in the pixel capacitor is transferred to a charge-sensitive amplifier. The bias voltage line is realized as a common front electrode for all sensor pixels. A photo of a sensor pixel before integrating the color sensor is shown in Fig. 2(b). The dashed box indicates the dimensions of the sensor pixel. The active area of the sensor is defined by the contact pad of the sensor, which occupies 67% of the total pixel area [Fig. 1(b)].

The actual color sensor is realized by an antiserial connection of two amorphous silicon nip diodes, which are integrated on top of the readout electronics. To planarize the readout transistors and to reduce the coupling between the optical sensor and the readout electronics, a 3- to 10-μm-thick oxynitride layer was prepared on top of the readout transistors before fabricating the sensor stack. Only the back contact and the n-layer of the optical sensor were patterned. The remaining layers of the sensor and the front electrode of the sensor array were unpatterned. Detailed descriptions of the deposition parameters and the device performance of amorphous silicon TFTs are given elsewhere [18]. The top contact of the sensor array is realized by radio frequency magnetron sputtered ZnO [19].

Different device designs can be used to optimize the spectral sensitivity of the color sensor. The optical bandgap and the thickness of the individual regions of the sensor have to be adjusted to match the color standards. The bandgap diagram of the optical sensor is shown in Fig. 3. The sensor consists of a top diode, which is penetrated at first by the incoming light. The absorber of the top diode has an optical bandgap of 2.2 eV. Therefore, blue light is absorbed in the top diode, whereas green and red light is transmitted through the top diode. The absorber of the bottom diode is divided into two regions. Region i_{II} of the bottom diode was realized by a silicon carbon layer with an optical bandgap of 1.9 eV, whereas the region i_{III} was formed by an intrinsic amorphous silicon layer. A very thin lightly n-type doped layer was introduced between the two absorption layers of the bottom diode. The thin layer leads to an increased electric field in region i_{II} of the bottom diode.

The spectral sensitivity of the sensor is changed by varying the applied bias voltage. Applying a positive voltage to the transparent conductive oxide (TCO) front electrode and the metal back contact of the nipin sensor leads to a reverse-biased top diode and a forward-biased bottom diode. The photocurrent of the sensor is determined by the photo-generated carriers in the top diode, whereas the photo-generated carriers in the bottom diode recombine. Therefore, the detector yields blue sensitivity. Changing the applied bias toward a negative voltage leads to a forward-biased top diode and a reverse-biased bottom

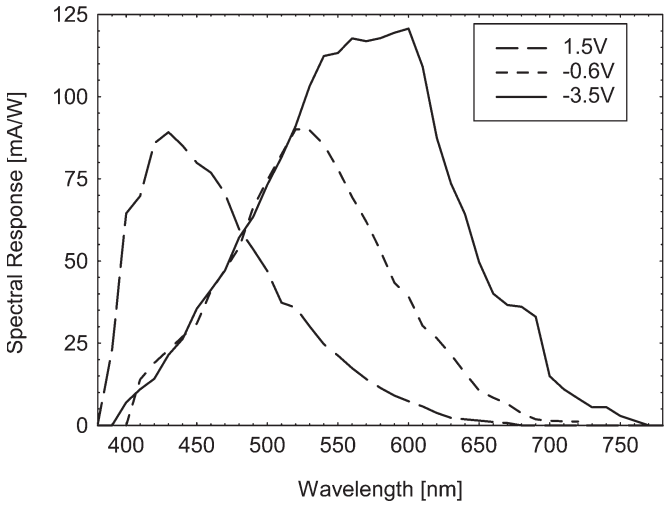

Fig. 4. Spectral response of the nipin sensors for the applied bias voltages of $V = +1.5, -0.6$, and -3.5 V.

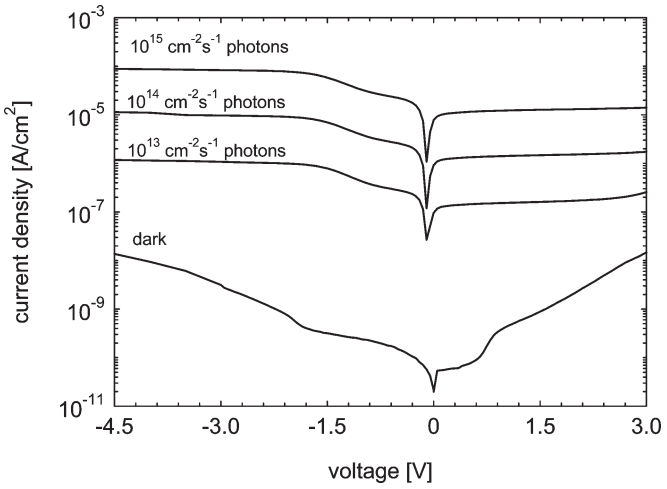

Fig. 5. $I-V$ characteristic of a nipin color sensor in the dark and under different illumination intensities.

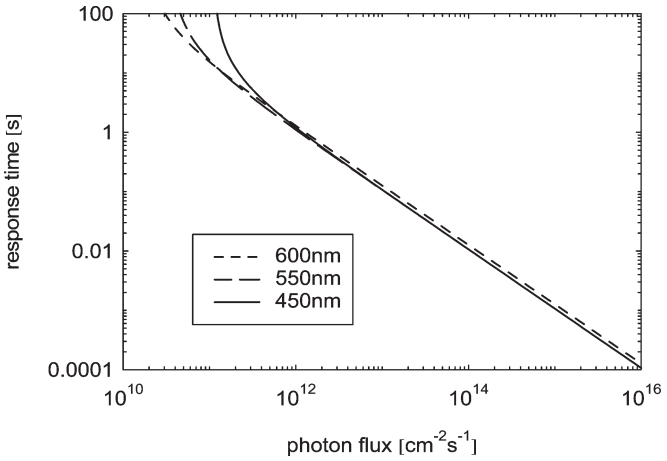

Fig. 6. Transient response time of the color sensor as a function of the photon flux.

diode. In this case, the sensor is green or green + red sensitive. For low negative voltages, the electric field in region i_{II} is much higher than the electric field in region i_{III}, so the photocurrent is determined by the photo-generated carriers in region i_{II}. For higher negative voltages, the electric field is enhanced throughout the entire bottom diode and the photocurrent is determined by the extracted carriers out of regions i_{II} and i_{III}.

III. Results

A. Color Sensor

The spectral sensitivity of the sensor array for different bias voltages is shown in Fig. 4. The maximum of the voltage-controlled spectral response of the nipin structure shifts from red to green and blue due to a change of the bias voltage from $V = -3.5$ V to $V = +1.5$ V. The bias voltage was applied to the common bias voltage electrode in Fig. 2(a). For a bias voltage of $+1.5$ V, the sensor exhibits a maximum of the spectral sensitivity at a wavelength of 430 nm. Applying a low negative voltage of -0.6 V to the optical sensor leads to a shift of the spectral sensitivity. In this case, the photocurrent is determined by the photo-generated carriers in region i_{II} of the bottom diode. The electric field in region i_{III} is not high enough to extract the photo-generated carriers out of this region. The sensor exhibits a maximum of the spectral response at wavelengths of 530 nm. For higher negative bias, almost all carriers can be extracted out of regions i_{II} and i_{III} and the spectral response shifts to 600 nm. The quantum efficiency of the optical sensor can be calculated by

$$QE(\lambda) = \mathrm{SR}(\lambda)\frac{hc}{e\lambda} \tag{1}$$

where $\mathrm{SR}(\lambda)$ is the spectral response, h is the Planck constant, e is the elementary charge, and λ is the wavelength of the incident light. The sensor exhibits quantum efficiencies of 0.25, 0.22, and 0.25 for the colors red, green, and blue (RGB).

To study the linearity, the dark performance, and the transient behavior of the color sensors, individual sensors were prepared on glass substrates. The current–voltage $(I-V)$ behavior of a sensor is given in Fig. 5. The sensor exhibits a dark current level of < 1 nA/cm^2 for the positive (+1.5 V) and small negative voltages (-0.6 V). For higher negative voltages (-3.5V), the dark current is increased up to 7 nA/cm^2. Furthermore, the photocurrent is plotted for different light intensities. During the measurement, the sensor was exposed to monochromatic light (red, 600 nm). Further measurements of the sensor show that the photocurrent of the sensor is linear over 4 orders of magnitudes [10]. The response time of the photocurrent of the sensor for different illumination conditions is given in Fig. 6. The total response time for an RGB sequence corresponds to the sum of the response times for red, green, and blue. The response time is inversely proportional to the level of intensity, so real-time imaging is not possible for low levels of intensity.

B. Sensor Array

Three images taken by the thin-film sensor array for different applied voltages are shown in Fig. 7(a)–(c). The array was operated by a readout electronic that transfers the readout

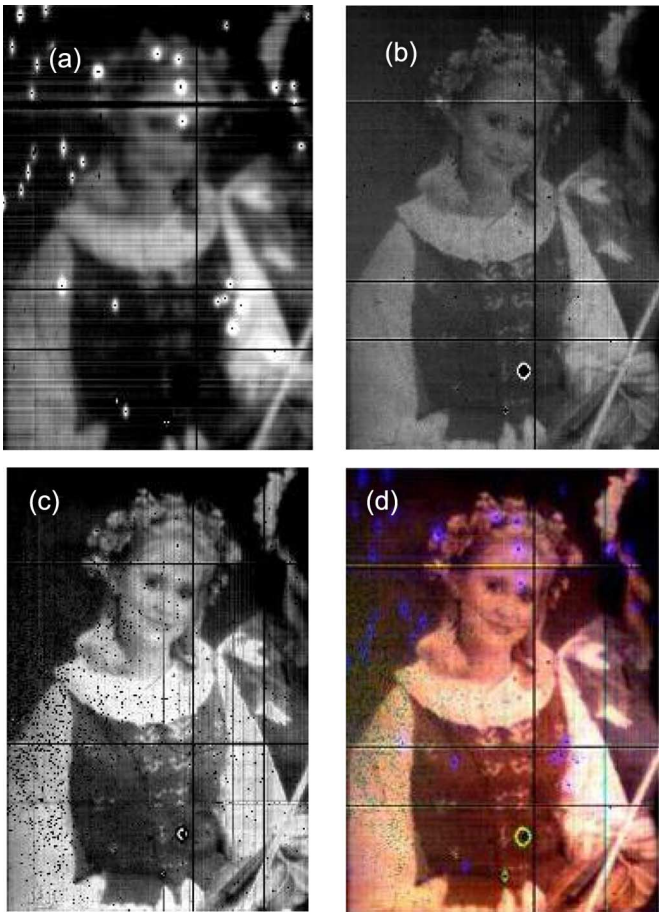

Fig. 7. Image taken by vertically integrated color sensor array for the voltages (a) +1.5, (b) −0.6, and (c) −3.5 V applied to the sensor. All three images have a resolution of 185 × 280 pixels. (d) Merged RGB image. (Color version available online at http://ieeexplore.ieee.org.)

signals to the sensor array and transfers the signal charges to external amplifiers and a 14-bit analog-to-digital converter. The readout electronics allows for operation of the array up to 20 Hz, with a dynamic range of 14 bits. The minimum electronic noise of the readout electronic is in the range of 1000–2000 electrons. The images in Fig. 7(a)–(c) correspond to the raw data taken by the sensor array. An integration time of 50 ms was used to readout each pixel. Due to the detection principle of the sensor, three frames had to be captured to acquire a complete color image. The images were taken for a photon flux of 100–1000 lx. All three images have a resolution of 185 × 280 pixels. The images were taken for different voltages of +1.5, 0.6, and −3.5V. For low negative voltages (−0.6 V), only the carriers were extracted from region i_{II} of the bottom diode [Fig. 7(b)]. Accordingly, the sensor is green sensitive. For high negative voltages, all photo-generated carriers in the bottom diode were extracted so that the sensor yields green + red sensitivity [Fig. 7(c)]. The red + green signals can be separated in the red and green signal by applying a color transform. The image in Fig. 7(a) was taken for an applied voltage of 1.5 V. In this case, only carriers generated in the top diode were extracted. The RGB color image is created by merging the chromatic images. A reference detailed description of the color analysis is given in [17].

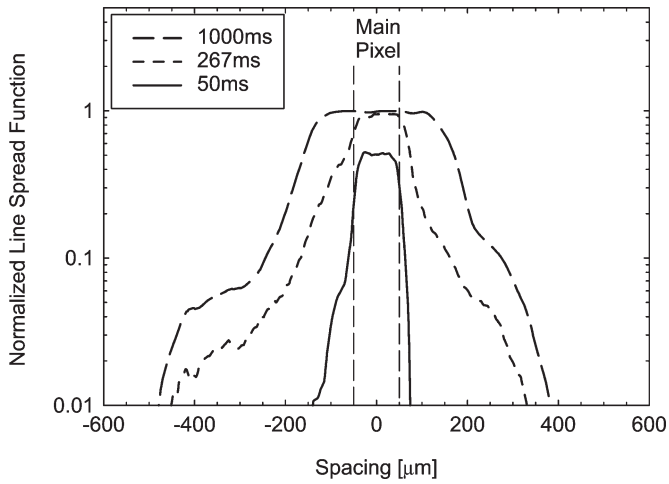

Fig. 8. Measured and normalized LSF of the bottom diode of the color sensor array for different integration times (50, 267, and 1000 ms). A voltage of −0.6 V was applied to the color sensor.

C. Pixel Crosstalk

A comparison of the images in Fig. 7 indicates a difference in contrast for the three images. The contrast of the image taken by the top diode of the color sensor array [Fig. 7(a)] is lower than the contrast of the two other images taken by the bottom diode [Fig. 7(b) and (c)]. The reduced image contrast is caused by pixel crosstalk.

To study the influence of pixel crosstalk on the image, contrast measurements of the line spread function (LSF) were carried out. The LSF was measured by placing a 15-μm slit directly on top of the sensor array. While measuring the LSF, the sensor array was exposed by a slide projector with projection optics. The intensity of the light source was controlled by neutral filters. During the measurement of the LSF, the intensity was in the range of 100–1000 lx.

The normalized LSF of the bottom diode is shown in Fig. 8. The LSF was measured for different integration times of the sensor array ranging from 50 to 1000 ms. The LSF is plotted as function of sensor spacing. A spacing of 0 μm corresponds to the center of the main pixel, which was exposed through the slit. The pixel pitch of the main pixel is indicated by dashed vertical lines in Fig. 8. Applying a voltage of −0.6 V to the sensor yields green sensitivity. Under such conditions, the bottom diode is reverse biased and the top diode is forward biased. For short integration times (50 ms), almost no spreading of the photo-generated charges is observed. The LSF is comparable to the LSFs measured for black/white sensor arrays using amorphous silicon nip diodes [18]. For longer integration times (276 and 1000 ms), the image starts to spread out. The pixels get saturated and the photo-generated charges start to spread into the neighboring pixels. For long integration times of 1000 ms, the charges were spread over four to five neighboring pixels. To illustrate the effect of charge spreading, a schematic cross section of the vertically integrated color sensor is shown in Fig. 9. The photo-generated charges spread from the exposed main pixel into the neighboring pixels because the multilayer stack is unpatterned except the n-layer of the bottom diode.

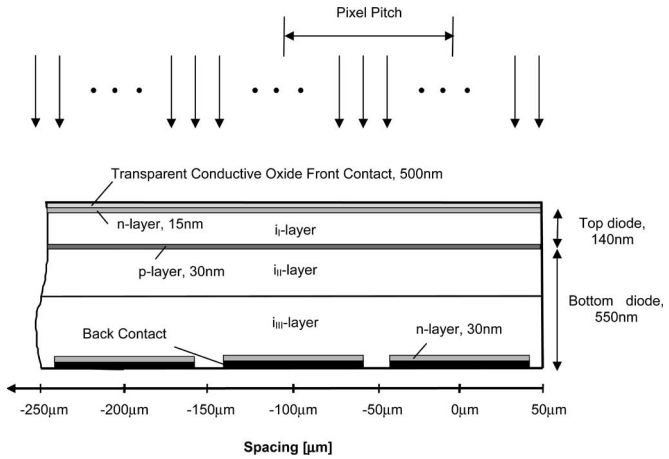

Fig. 9. Schematic cross section of the color sensor integrated on top of the readout electronics.

Another measure of the image contrast is the modulation transfer function (MTF). The MTF is the Fourier transform of the point spread function (PSF), or in one-dimension (1-D) the LSF. In the ideal case, the 1-D MTF can be described as light transmitted through a very narrow aperture (delta function), which is sampled by a pixel (rectangular function). An expression for the normalized LSF is given as

$$\mathrm{LSF}(x) = \delta(x) * \mathrm{rect}\left(\frac{x}{d}\right) \tag{2}$$

where d is the pixel pitch. The Fourier transform of the LSF leads to

$$\mathrm{MTF}(f) = \Im\left(\mathrm{LSF}(x)\right) = \sin c(\pi df) \tag{3}$$

where $f = 1/x$ is the spatial frequency. The MTF has the value of unity at spatial frequencies of zero, and decreases to zero at higher frequencies. In the case of an ideal imager, the MTF is high for frequencies below the Nyquist frequency and low for spatial frequencies above the Nyquist frequency. The Nyquist frequency is given by $f_N = 1/2d$. However, the color sensor array exhibits image spreading, so the measured MTF deviates from the ideal MTF given in (3). To account for the spreading of the charges in the sensor, the MTF was extended in the form of

$$\mathrm{MTF}(f) = \sin c(\pi df)\frac{1}{1+\alpha f^2}. \tag{4}$$

The additional term considers spreading of the pulses in the x-direction (perpendicular to the incident light), where α is a spreading coefficient. The measured MTF of the bottom diode for -0.6 V is shown in Fig. 10. Two MTFs are given for short [Fig. 10(a)] and long [Fig. 10(b)] integration times. For short integration times (50 ms), the MTF is very close to the ideal MTF determined by the pixel pitch. The measured MTF slightly deviates from the ideal MTF shown in Fig. 10(a). Longer integration times (1000 ms) lead to spreading of the photo-

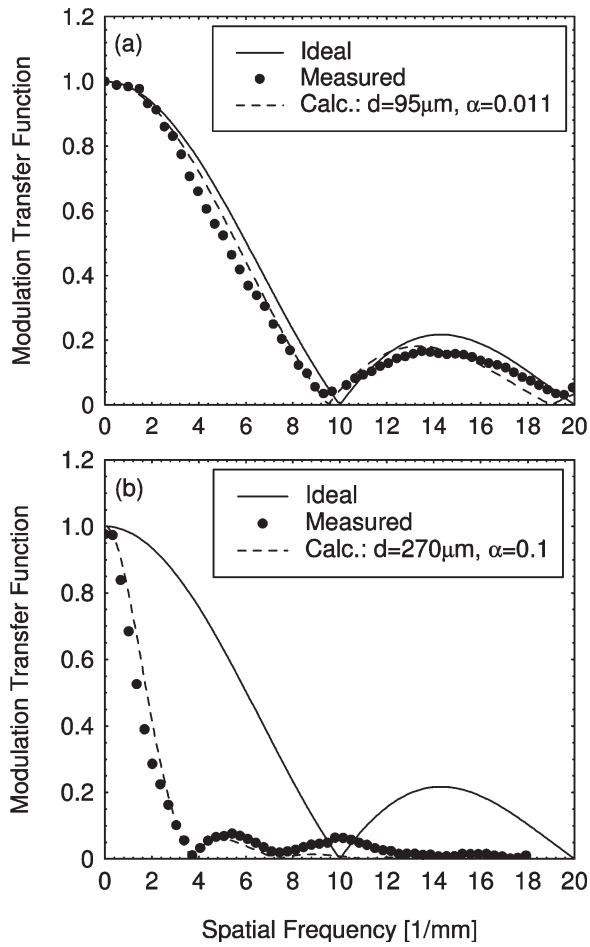

Fig. 10. Measured and calculated MTF of the bottom diode of the color sensor array for short (50 ms, top) and long integration times (1000 ms, bottom). A voltage of -0.6 V was applied to the color sensors.

generated charges, so the effective pixel pitch is increased. To fit the experimental data by (4), the pixel pitch had to be increased to an effective pixel pitch of 270 μm [Fig. 10(b)].

Increasing the applied bias voltage of the color sensor from -0.6 V to -3.5 V leads to a slight increase of the charge spreading in the multilayer stack. This is observed for short integration times (50 ms) and long (1000 ms) integration times, although the effect is more pronounced for longer integration times.

The crosstalk behavior of the bottom diode is quite different from the behavior of the top diode. The normalized LSF of the top diode for different integration times is shown in Fig. 11. Although the pixel is not saturated for an integration time of 50 ms, a distinct spreading of the charges into the neighboring pixels is already observed. The effect is even more pronounced for longer integration times (267 and 1000 ms). Hence, the MTF of the top diode deviates from the ideal MTFs even for short integration times. The ideal MTF and the fit of the measured MTF are shown in Fig. 12(a) and (b). For short integration times of 50 ms, the measured curve can only be described by increasing the spreading coefficient to 0.18. For longer integration times, the spreading coefficient stays the same, but the effective pixel pitch had to be increased to 320 μm to describe the measurement.

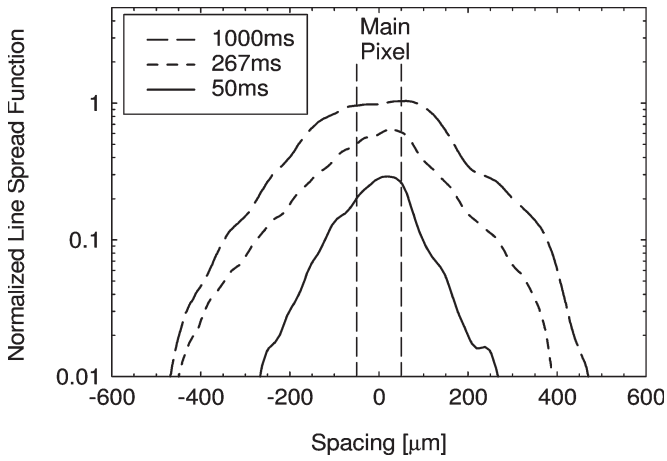

Fig. 11. Measured and normalized LSF of the top diode of the color sensor array for different integration times (50, 267, and 1000 ms). A voltage of +1.5 V was applied to the sensor array.

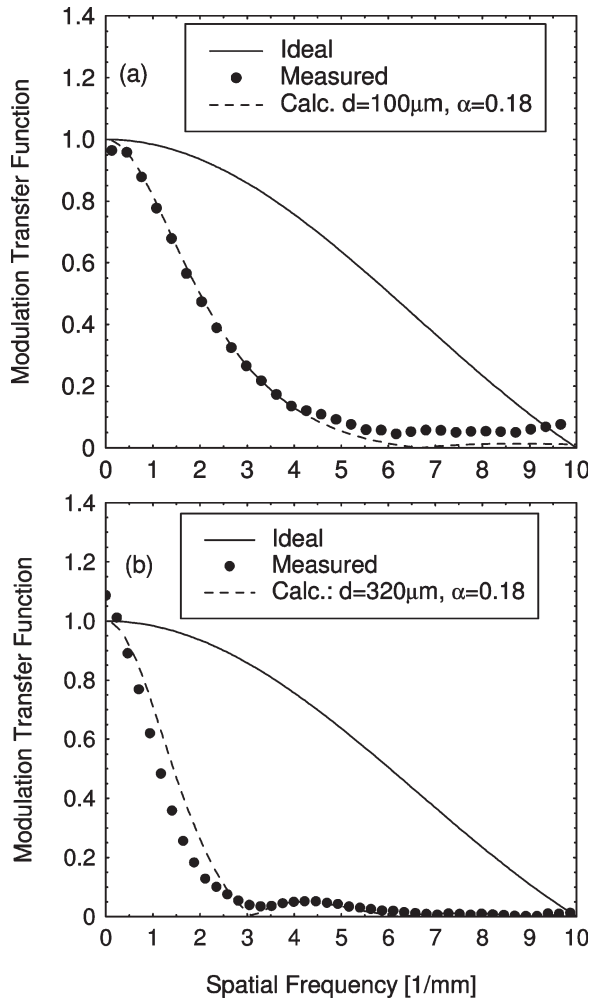

Fig. 12. Measured and calculated MTF of the top diode of the color sensor array for short (50 ms, top) and long integration times (1000 ms, bottom). A voltage of +1.5 V was applied to the color sensors.

IV. Discussion

The vertical integration of the color channels facilitates the realization of color Moiré or color aliasing free sensors. Different concepts can be applied to detect the color information in the depth of the device structure. In this study, a two-terminal color sensor was deployed, which varies the spectral sensitivity as a function of the applied bias voltage. Color sensors based on two terminals are characterized by a sequential read-out process, whereas color sensors based on stacked diodes allow for the readout of all channels at the same time. Furthermore, the spectral sensitivities of stacked color sensors are closer to the spectral sensitivities of the human eye, which reduce the color error of the sensor [21]. The spectral sensitivities of the nipin sensor (Fig. 4) exhibits a considerable overlap. Such an overlap can lead to a significant increase of the color error. However, calculations of the color error reveal that the color error is comparable to standard CFA-based sensor arrays [17]. This can be achieved by an optimized device design of the sensor. On the other hand, the significant overlap leads to an increase of the noise level when transforming the sensor signal to a standard color space.

In terms of the integration of optical sensors with the readout electronics, the stacked sensor is distinctly more complex. Due to the distinctly more complex integration of stacked sensors and readout electronics, the area fill factor of such sensor arrays is reduced. The area fill factor of two-terminal devices, however, can be very high. In particular, if the thin-film sensors are unpatterned. A cross section of such a structure is shown in Fig. 9. The area fill factor for the presented sensor structure is larger than 67%. Furthermore, the sequential readout scheme leads to color errors due to the movement of the object within a color frame (red, green and blue). The error can only be minimized by reducing the integration time and/or increasing the frame rate. However, the achievable frame rate is limited for low levels of intensity. Such a problem can only be prevented by the vertical stacking of the three sensors for red, green, and blue.

Image lag is another important factor that has to be considered when designing a color sensor array. In our case, the image is limited by the top diode. The behavior of the bottom diode is comparable to black/white image sensor arrays. A detailed analysis of the image lag of a two-color sensor based on a pinip structure is given in [16]. The nipin three-color sensor and the pinip two-color sensor exhibit a similar behavior. The image lag is caused by the transient behavior of the two-terminal color sensors.

Image contrast, which determines the image quality, is another important factor. The unpatterned thin-film sensor stack leads to a reduced contrast of the sensor array. In particular, the top diode of the color sensor exhibits a distinct reduction of the image contrast. Blooming of the pixels is observed independent of the integration times. Even for short integration times, the charges start to spread out. This behavior can be attributed to the fact that the entire top diode is unpatterned. The increased pixel crosstalk is caused by an electric field gradient along the p-layer of the sensor. For example, illuminating the sensor arrays through a very narrow aperture leads to a distinct change of the electrical field distribution in the exposed area of the sensor. The exposure causes a decrease of the built-in voltage for both of the diodes (top and bottom diode) of the color sensor. A schematic band diagram of the sensor in the dark and under illumination conditions is shown in Fig. 13. The reduction of

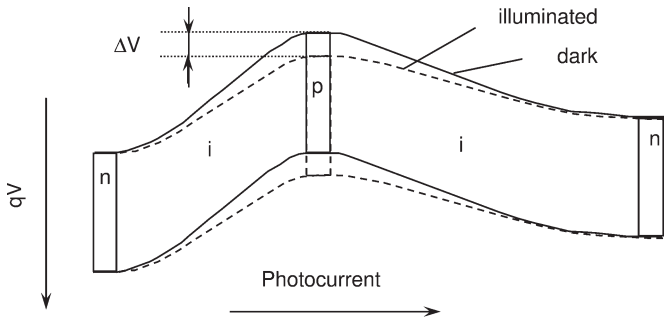

Fig. 13. Schematic band diagram of the nipin color sensor in the dark (solid line) and under illumination (dashed line) for a positive applied bias voltage.

the built-in potential is caused by the filling of defect states in the vicinity of the p-layer. In the dark, these defects are neutral. Under illumination, these defects get positively charged, which reduces the built-in potential. As a consequence, the electric potential in the p-layer of the sensor structure is reduced. Therefore, a spatial variation of the light intensity leads to an electric field gradient along the p-layer, which causes the charges to spread out from the exposed main pixel into the neighboring pixels. Depending on the illumination conditions, the electric potential in the p-layer can be changed by up to 150 mV. A more detailed description of the device behavior under different illumination intensities is given elsewhere [22].

To reduce the pixel crosstalk and to increase the image contrast, several strategies can be followed. The thickness and the doping concentration of the p-layer of the nipin color sensor can be reduced. However, the p-layer is already very thin. A further reduction of the p-layer thickness is not possible. As an alternative, the complete layer stack or parts of the layer stack can be patterned. Furthermore, patterning of the entire layer stack leads to a significant reduction of the area fill factor. However, patterning of the entire sensor stack requires the deposition of an additional insulation layer, which separates individual pixels from each other. Such an additional insulation layer is needed as the front electrode of the sensor (Fig. 3) is used as a common electrode for all sensor elements.

Therefore, it seems to be the most promising approach to pattern only parts of the sensor stack. Patterning of the p-layer will be the best solution as the pixel crosstalk is caused by the unpatterned p-layer. As the p-layer is very thin in comparison to the entire layer stack, no other measures have to be taken. A planarization of the sensor before preparing the transparent front electrode is not necessary. As a consequence, pixel crosstalk will be reduced and the MTF will be improved while maintaining the high area fill factor.

V. Conclusion

For the first time, a Moiré effect or color aliasing free large-area three-color sensor array was realized. The sensor array was fabricated on glass substrates with a resolution of 512 × 512 pixels. The optical sensor and the readout transistors of the sensor array were realized by amorphous silicon and its alloys at deposition temperatures below 300 °C. The sensor array enables color Moiré-free color detection. Accordingly, the complete color information can be detected at the same position of a sensor array without using optical filters. The color detector is based on the antiserial connection of two amorphous diodes. The spectral sensitivity of the sensor can be varied by changing the applied bias voltage. The blue color information is detected by the top diode for positive voltages, and green and red sensitivity by the bottom diode for negative voltages. Furthermore, image quality was analyzed by measuring the normalized LSF and the MTF of the sensor array for different voltages and integration times. The image contrast of the blue image is reduced in comparison to the contrast of the red and the green images. The contrast of the blue image—detected by the top diode—is reduced due to a change of the electric potential in the p-layer of the sensor as a consequence of light exposure. The change of the electric potential leads to a spreading of the charges in the sensor.

Acknowledgment

The authors would like to thank B. Rech, F. Finger, and their research groups at the Research Center Jülich for their support in preparing the color sensors and the team of the process line at the Palo Alto Research Center for providing the TFT backpanel.

References

[1] B. E. Bayer, "Color imaging array," U.S. Patent 3 971 065, Jul. 20, 1976.
[2] A. S. Glassner, *Principles of Digital Image Synthesis*, vol. 1/2. San Mateo, CA: Morgan Kaufmann, 1995.
[3] R. B. Mirell, "Color separation in an active pixel cell imaging array using a triple-well-structure," U.S. Patent 5 965 865, Oct. 12, 1999.
[4] P. Seitz, D. Leipold, J. Kramer, and J. M. Raynor, "Smart optical and image sensors fabricated with industrial CMOS/CCD semiconductor processes," *Proc. SPIE*, vol. 1900, pp. 21–30, 1993.
[5] D. P. Poenar and R. F. Wolfenbuttel, "Thin-film optical sensors with silicon compatible materials," *Appl. Opt.*, vol. 36, no. 21, pp. 5109–5121, Jul. 1997.
[6] K. Eberhardt, T. Neidlinger, and M. Schubert, "Three color sensor based on amorphous nipin layer sequence," *IEEE Trans. Electron Devices*, vol. 42, no. 10, pp. 1763–1768, Oct. 1995.
[7] J. Zimmer, D. Knipp, H. Stiebig, and H. Wagner, "Amorphous silicon based unipolar detector for color recognition," *IEEE Trans. Electron Devices*, vol. 46, no. 5, pp. 884–891, May 1999.
[8] P. Rieve, M. Sommer, M. Wagner, K. Seibel, and M. Böhm, "a-Si:H color imagers and colorimetry," *J. Non-Cryst. Solids*, vol. 266–269, pp. 1168–1172, May 2000.
[9] H. Stiebig, J. Giehl, D. Knipp, P. Rieve, and M. Böhm, "Amorphous silicon three color detector," in *Proc. Mater. Res. Soc. Symp.*, 1995, vol. 377, pp. 517–522.
[10] D. Knipp, H. Stiebig, J. Fölsch, F. Finger, and H. Wagner, "Amorphous silicon based nipin structure for color detection," *J. Appl. Phys.*, vol. 83, no. 3, pp. 1463–1468, Feb. 1998.
[11] F. Palma, *Multilayer Color Detectors*, vol. 37, R. A. Street, Ed. Berlin, Germany: Springer-Verlag, 2000, pp. 306–338.
[12] R. F. Lyon and P. M. Hubel, "Eyeing the camera: Into the next century," in *Proc. 10th Color Imag. Conf.: Color Sci. Eng. Syst. Technol. Appl.*, Scottsdale, AZ, Nov. 2002, pp. 349–355.
[13] B. Schneider, P. Rieve, and M. Böhm, "Image sensors in TFA (thin film on ASIC) technology," in *Handbook of Computer Vision and Applications*. Boston, MA: Academic, 1998.
[14] T. Lulé, M. Wagner, M. Verhoeven, H. Keller, and M. Böhm, "100 000-pixel-120-dB imager in TFA technology," *IEEE J. Solid-State Circuits*, vol. 35, no. 5, pp. 732–739, May 2000.
[15] S. Benthien, T. Lulé, B. Schneider, M. Wagner, M. Verhoeven, and M. Böhm, "Vertically integrated sensors for advanced imaging applications," *IEEE J. Solid-State Circuits*, vol. 35, no. 7, pp. 939–945, Jul. 2000.
[16] M. Mulato, F. Lemmi, J. Ho, R. K. Lau, J. P. Lu, and R. A. Street, "Two-color amorphous silicon image sensor," *J. Appl. Phys.*, vol. 90, no. 3, pp. 1589–1599, Aug. 2001.

[17] D. Knipp, R. A. Street, H. Stiebig, M. Krause, J.-P. Lu, S. Ready, and J. Ho, "Vertically integrated thin film color sensor arrays for imaging applications," *Optics Express*, vol. 14, no. 8, p. 3106, Apr. 2006.
[18] R. A. Street, *Large Area Image Sensor Arrays*, vol. 37, R. A. Street, Ed. Berlin, Germany: Springer-Verlag, 2000.
[19] O. Kluth, A. Löffl, S. Wieder, C. Beneking, L. Houben, B. Rech, H. Wagner, S. Waser, J. A. Selvan, and H. Keppner, "Texture etched Al-doped ZnO: A new material for enhanced light trapping in thin film solar cells," in *Proc. IEEE 26th PVSEC*, 1997, pp. 715–718.
[20] W. Luft and Y. Tuso, *Hydrogenated Amorphous Silicon Alloy Deposition Processes*. New York: Marcel Dekker, 1993.
[21] P. G. Herzog, D. Knipp, H. Stiebig, and F. König, "Colorimetrical characterization of novel multiple-channel sensors for imaging and metrology," *J. Electron. Imaging*, vol. 8, no. 4, pp. 342–353, Oct. 1999.
[22] B. Stannowski, H. Stiebig, D. Knipp, and H. Wagner, "Transient photocurrent of three-color detectors based on amorphous silicon," *J. Appl. Phys.*, vol. 85, no. 7, pp. 3904–3911, Apr. 1999.

Dietmar Knipp (M'03) received the M.S. degree from the University Siegen, Siegen, Germany, in 1995 and Ph.D. degree from the Technical University Aachen, Aachen, Germany, in 1999, both in electrical engineering.

From 1996 to 2000, he was with the Research Center Jülich, first as a Research Assistant, and then as a Postdoctoral Scientist, working on amorphous and nanocrystalline silicon and its application for optical sensors. From 2000 to 2002, he was with the Palo Alto Research Center, Palo Alto, CA, where he carried out research on organic and molecular electronics. He was a Senior Researcher at the Interuniversity Microelectronic Center, Leuven, Belgium, working in the area of Advanced Components and Sensor Systems. In 2003, he joined the International University Bremen, Bremen, Germany, as an Assistant Professor of electrical engineering. His research focuses on electronic devices and photonics, with particular emphasis on organic and molecular transistors, nanophotonics, and optical sensor technologies.

Robert A. Street, photograph and biography not available at the time of publication.

Helmut Stiebig received the Ph.D. degree in electrical engineering from the Aachen University of Technology, Aachen, Germany, in 1997.

Since 1992, he has been with the Institute of Photovoltaics, Research Center Jülich, Jülich, Germany. He is currently the Head of a research group on "device analysis and sensor technology." His research interests include the investigation of the optoelectronic properties of amorphous and microcrystalline silicon and related materials, development of innovative device structures for solar cell applications, device analysis and numerical modeling, and the development of optical sensors based on thin-film technology.

Mathias Krause, photograph and biography not available at the time of publication.

Jeng-Ping Lu, photograph and biography not available at the time of publication.

Steve Ready, photograph and biography not available at the time of publication.

Jackson Ho, photograph and biography not available at the time of publication.